ARTICLE TYPE

How does iron interact with sporopollenin exine capsules? An X-ray absorption study including microfocus XANES and XRF imaging

Stephen J. Archibald,[a] Stephen L. Atkin,[b,c] Wim Bras,[d] Alberto Diego-Taboada,[b,c] Grahame Mackenzie,[a,c] J Frederick W. Mosselmans,[e] Sergey Nikitenko,[d] Paul D. Quinn,[e] Michael F. Thomas[f] and Nigel A.
5 **Young*[a]**

Sporopollenin exine capsules (SECs) derived from plant spores and pollen grains have been proposed as adsorption, remediation and drug delivery agents. Despite many studies there is scant structural data
10 available. This X-ray absorption investigation represents the first direct structural data on the interaction of metals with SECs and allows elucidation of their structure-property relationships. Fe K-edge XANES and EXAFS data have shown that the iron local environment in SECs (derived from *Lycopodium clavatum*) reacted with aqueous ferric chloride solutions is similar to that of ferrihydrite (FeOOH) and by implication ferritin. Fe K_α XRF micro-focus experiments show that there is a poor correlation between the
15 iron distribution and the underlying SEC structure indicating that the SEC is coated in the FeOOH material. In contrast, the Fe K_α XRF micro-focus experiments on SECs reacted with aqueous ferrous chloride solutions show that there is a very high correlation between the iron distribution and the SEC structure, indicating a much more specific form of interaction of the iron with the SEC surface functional groups. Fe K-edge XANES and EXAFS data show that the Fe^{II} can be easily oxidised to give a structure
20 similar to, but not identical to that in the Fe^{III} case, and that even if anaerobic conditions are used there is still partial oxidation to Fe^{III}.

Introduction

The use of microcapsules for drug (and other actives) delivery is of increasing importance. Polymer constructs, hydrogels and hybrid
25 capsules have been investigated with materials including natural polymers (e.g. chitosan, alginates etc.), biodegradable synthetic polymers (e.g. polypeptides, polyesters etc.) and mesoporous silica constructs.[1-3] These materials can be used to form nanoparticles, vesicles, liposomes or polymer conjugates which allow delivery and controlled release of payloads to biological systems. The mechanism for guest molecule entry/release in molecular capsules and the form in which it is retained can be particularly important to effective drug delivery or catalyst activity.[4,5]

30

Whilst the manufacture of synthetic microcapsules can be challenging in terms of uniformity of size, chemical structure, morphology, chemical and physical resistance etc., nature has developed a range of microcapsules that are ideally suited to this task. In particular, the exoskeletal shells (exines) derived from plant spores and pollen are especially attractive since they range from 4 μm for *Myosotis* (forget-me-not) to 250 μm for *Cuburbita* (pumpkin). Particular features of these exines are that they are constructed from sporopollenin, a highly
35 cross-linked organic polymer of approximate composition $C_{90}H_{144}O_{27}$ [6] which has remarkable physical, chemical and biological stability. For example, intact exines have been recovered from 500 million year old sedimentary rocks.[7] The exines are hollow and their *ca.* 2 μm thick walls are perforated with numerous channels which make them porous so that both the outer and inner surfaces are potentially available for binding, which in turn lends them to a wide variety of applications as microcapsules, robust solid supports, and in some cases both. The combined inertness and robustness of the sporopollenin exine capsules (SECs), especially to conditions within the gastrointestinal
40 tract,[8,9] makes them very attractive as delivery agents for pharmaceuticals and other actives[8,9,28,29] and medical imaging.[10] They have also been used for solid phase peptide synthesis,[11,12] as micro-reactors for the preparation of nanoparticles,[13] and as solid supports for palladium catalysed Heck reactions.[14] Functionalised SECs with either carboxylated or glyoximated diamino groups have been used for ion exchange and ligand exchange chromatography,[15-30] often in conjunction with Co.[16,17,19-21,24-30] The SECs have also been proposed for metal remediation and adsorption either on their own[31,32] or functionalised with carboxylate and glyoxime groups,[18,33] dithiocarbamates,[34]
45 glutaraldehyde,[35] (*E*)-4-((2-hydroxyphenylimino) methyl) benzoic acid,[36] Schiff bases,[37-41] or calixarenes.[42,43] Magnetized pollen grains

(ragweed with magnetite prepared from $FeCl_2$ and $FeCl_3$) have been proposed as a method for the removal of organic pollutants from aqueous media,[44] and those derived from *Candida rugosa* have shown excellent enatioselectivity.[45,46]

Despite the large amount of work carried out on metal sorption and coordination to SECs there are very few reports on the nature of the interaction between the metal ions and the sporopollenin itself. It is important to understand how such conjugates are capable of fulfilling their roles to enable insights into new potential applications such as solid supports for metal catalysts. X-ray absorption spectroscopy (XAS) is able to probe the local structural environment around the element of interest. When carried out using micro-focus instrumentation it can provide both structural and chemical state imaging data from single exines. This approach has been used previously at the Fe K-edge to study geological[47-51] and soil samples,[52,53] archaeological specimens,[54-59] biological tissues[60-68] and cometary material.[69-72] Whilst there has been some X-ray absorption work on sporopollenin using the C K-edge (*ca.* 290 eV), which identified ketonic groups on the surface of the pollen grain and aliphatic carbon across the whole structure,[73] there appears to be no XAS experiments carried out at the metal K-edges in the literature. In this work we report an Fe K-edge XANES and EXAFS as well as an Fe K_α X-ray fluorescence and Fe K-edge XANES imaging investigation of sporopollenin reacted with iron under a variety of conditions.

As part of a larger investigation into the use of SECs for drug delivery [8,9,13,74-77] and other applications [6,10,78-81] we have carried out this study on the interaction of iron with SECs to explore the structure-property relationships and whether they could be used as a vehicle for iron delivery. In particular, do the known redox properties of sporopollenin[79,82] play a role in stabilising iron(II) in the form of a conjugate for iron bio-availability? Iron-deficiency anaemia is a major cause of morbidity and mortality worldwide and affects a large proportion of children in many developing countries.[83] An effective, stable and inexpensive formulation to deliver iron(II) with increased bioavailability has potential advantages over more traditional iron(II) formulations.[84]

Experimental

The preparation of the SECs has been described in detail previously,[8,75] but briefly the sporoplasm and cellulose intine of the *Lycopodium clavatum* raw spores were removed using successive treatments of hot acetone, potassium hydroxide and phosphoric acid. The iron(II) and iron(III) samples were prepared using a suspension of SECs (2.0 g) in water (50mL) with either iron (III) chloride (4.0 g) or iron (II) chloride tetrahydrate (4.0 g) which was stirred at room temperature for 3h. Particles were recovered by filtration, washed with water (3×50 mL), ethanol (2×50 mL) and acetone (50 mL), and air dried (*ca.* 1-2 h) to constant weight. Iron(II) samples were also prepared by an analogous method under an inert atmosphere using standard Schlenk techniques. Dry, degassed solvents were used and the reaction with the iron(II) salts was carried out in a Schlenk tube with stirring at r.t. Argon was used as the inert gas for sample synthesis and filtration. The vacuum dried samples were stored under argon and transported in the Schlenk tubes to the synchrotron beam line. At the synchrotron the samples were handled in a glove bag. The basic ferric acetate, ferrous acetate and cobalt acetate tetrahydrate were used as supplied by the manufacturers.

The amount of iron incorporated on the SECs was determined by ICP-OES (Perkin Elmer Optima 5300DV) and the SEM images were obtained using a Zeiss EVO 60 instrument.

Bulk Fe K-edge and Co K-edge XANES and EXAFS spectra were collected in transmission mode on the BM26A DUBBLE XAFS beamline at the ESRF using a double crystal Si(111) sagittal focussing monochromator.[85] Harmonic rejection was obtained using mirrors. The samples were presented as 13 mm pressed discs. The micro-focus XRF and XANES data were obtained from beamline I18 at the Diamond Light Source using a Si(111) double crystal monochromator and Kirkpatrick-Baez (KB) mirrors to give a spot size of ca 2.3 x 2.3 μm.[86] The fluorescence data were collected with a 9 element C-train Ge detector using the Xspress-2 data processing system. Bulk Fe K-edge XANES and EXAFS were also obtained in transmission mode from beamline I18 at the Diamond Light Source using the Si(111) double crystal monochromator and in this case the beam size was increased to *ca.* 100 μm by overbending the KB mirrors.[86] In both cases the samples were presented mounted between Mylar sheets.

The XAS spectra were calibrated using the first maximum in the first derivative spectrum of either an iron (7112.0 eV) or cobalt (7709.0 eV) foil.[87] The X-ray absorption spectra were averaged using Athena,[88] and background subtracted using either PAXAS[89] or Pyspline[90] with a quadratic pre-edge function and splines for the post-edge. The edge positions in the XANES spectra were defined as the energy corresponding to a normalised absorbance of 0.5. The k^3-weighted EXAFS spectra were modelled using Excurv98.[91] The XRF images were processed using PyMCA.[92]

Mössbauer data were obtained using a conventional constant acceleration Mössbauer spectrometer incorporating a ~ 25 mCi source of ^{57}Co in a Rh matrix. The ^{57}Fe Mössbauer chemical/isomer shift data are quoted relative to metallic iron at room temperature.

Results and Discussion

Physical characterisation of the SECs

ARTICLE TYPE

The SEM images of the *Lycopodium clavatum* SECs after reaction with ferric and ferrous chloride solutions shown in Figure 1. These images are essentially identical to those of unreacted SECs reported by us previously,[10,13,75,78,81] indicating no significant change in the structure or morphology of the SECs on iron loading. The SEM images reveal that the SECs are approximately 25 μm in diameter with a hemispherical cap ending in a trilete structure on the underside, and that they remain hollow after reaction with the metal solutions. Typical
5 surface areas are 4 m^2 g^{-1} with a shell thickness of 2-3 μm.[8,78] The surface is known to be continuous with large portholes (1 -2 nm diameter)[93] as well as nano-sized channels.(15 – 20 nm).[94]

The iron loading of the SECs prepared from $FeCl_3$ aqueous solutions and air dried was *ca.* 6 mg g^{-1}, whereas for the samples prepared from $FeCl_2$ aqueous solutions and air dried, values of *ca.* 30 mg g^{-1} were obtained. When anaerobic (Schlenk) techniques were used with
10 $FeCl_2$ solutions, loadings of *ca.* 12 mg g^{-1} were observed, but when $Fe(BF_4)_2$ solutions were used, much lower values of *ca.* 2 mg g^{-1} were obtained. Preliminary experiments have shown that the amount of iron released in simulated gastric fluid at 37°C from the air dried SECs prepared from aqueous $FeCl_2$ solutions was *ca.* 13.5% after 1 hour, *ca.* 21% after two hours and *ca.* 37% after 6 hours.

The chemical structure of sporopollenin has not been fully elucidated for any plant species due to its complexity, but it is known to be a
15 highly cross-linked organic polymer with long aliphatic chains, conjugated phenols, hydroxyls, ethers, methyls and carboxylic acids.[75] Elemental analysis for the SECs used in this work have been previously reported (%C, 62.1 ± 0.5; %H 7.3 ±0.3; %N 0.1 ± 0.1),[74] giving an approximate composition of $C_{90}H_{144}O_{27}$.[6] XRD patterns obtained from SECs are known to contain very broad peaks.[8]

Fe K-edge X-ray absorption spectroscopy

20 Fe K-edge XANES data can yield information about both the oxidation state of the iron as well as its coordination environment. The edge position is very sensitive to oxidation state and is at higher energy for higher oxidation states. The pre-edge features, which are often labelled 1s-3d, are sensitive to oxidation state, and their relative intensity can be used diagnostically to identify different coordination geometries.[95] Although the 1s-3d transitions are formally forbidden, the pre-edge peaks have some intensity due to quadrupole transitions, as well as relaxation of the Laporte and orbital selection rules.
25

To help identify the oxidation states and coordination geometry of the iron in the SECs, a selection of spectra from model compounds were also obtained. In particular, those of Fe^{II} and Fe^{III} acetate as carboxylate groups have been shown to be part of the SEC structure.[80] The iron is in an octahedral environment in both cases, but in basic ferric acetate the structural motif is tri-nuclear,[96-98] whereas in ferrous acetate it is a 2D coordination polymer.[99] The Fe K-edge XANES spectra of basic ferric acetate (Fig. 2(a)) and ferrous acetate (Fig. 2(g)) indicate
30 that there is a shift of *ca.* 4 eV in the edge position between the two oxidation states (7124.5 eV (Fe^{III}) and 7120.6 eV (Fe^{II})) and this is consistent with previous work.[54,55,71,72,100,101] In contrast, there is a smaller shift of *ca.* 1.5 eV in the position of the pre-edge peaks, which again is consistent with the literature data.[95,100]

Comparison of the Fe K-edge XANES spectra of ferric acetate (Fig. 2(a)) with those of the SEC samples prepared from ferric chloride
35 (Fig. 2(b)) and ferrous chloride solutions (Fig. 2 (c)) followed by air drying, confirm that both of these spectra are consistent with octahedral Fe^{III}. In particular, the Fe K-edge XANES spectra of the SECs in Figs. 2(b) and (c) are very similar to those observed for horse spleen ferritin[52,60,102-107] and frataxin.[103] Although the iron core of ferritin is usually assumed to be ferrihydrite-like (amorphous or short range ordered FeOOH),[108-111] there is evidence that it has a polyphasic structure comprising ferrihydrite, magnetite and hematite,[105,112] hence comparison with both the iron oxides and oxyhydroxides is required. There have been extensive Fe K-edge XANES investigations of both
40 the iron oxides [wüstite (FeO),[101,113] hematite (α-Fe_2O_3),[52,70,72,100,103,113-119] maghemite (γ-Fe_2O_3),[57,113,115-117,120,121] magnetite (Fe_3O_4),[57,60,70,71,103,113,116,117,120-122]] and the iron oxyhydroxides [goethite (α-FeOOH),[52,70,72,100,103,114,116,118,121-123] akaganéite, (β-FeOOH),[53,56,101,114,119,122] lepidocrocite, (γ-FeOOH)[52,100,116,121,122,124] as well as the less ordered ferrihydrite [52,56,57,71,72,100,101,114,116-119,122,125,126] and feroxyhyte.[57]].

45 The edge structures in Figs. 2(b) and (c) are more similar to all of the iron oxyhydroxide materials rather than the iron oxides. Whilst Konishi *et al.* have compared directly the Fe K-edge XANES data for the α-, β-, and γ-FeOOH materials and the nearest resemblance to those in Fig. 2(b,c) is akaganéite,[122] the SEC data most closely resemble those of 2 line and 6 line ferrihydrite[53,58,100,116-118,121,125] (the labelling refers to the number of diffraction peaks observed in X-ray powder diffractograms) rather than goethite (α-FeOOH),[53,73,100,114,116,118,121,122,126] akaganéite (β-FeOOH),[56,57,101,114,119,122] or lepidocrocite (γ-FeOOH).[53,116,121,122]
50

The pre-edge features in Fig. 2(b) and (c) are very similar to those observed for ferrihydrite as they are only comprised of one peak in both the absorbance and 1st derivative spectra.[57,121] In contrast, in goethite[52,72,100,127] and lepidocrocite[53] two clearly resolved 1s-3d pre-edge

features are observed.[52,72,100,127] The spectra of akaganéite have one pre-edge feature in some reports,[56,101,119] and two in others.[55,114] It has also been reported that the hydrolysis of ferric chloride solutions with lower OH/Fe ratios give rise to a single peak in the pre-edge region rather than two.[114]

5　Preliminary ^{57}Fe Mössbauer data of the air dried SECs prepared from ferrous chloride solution revealed a quadrupole doublet with an isomer shift of 0.49 mm s^{-1} and a quadrupole splitting of 0.68 mm s^{-1}, consistent with the presence of paramagnetic, octahedral Fe^{III}. In addition, the lack of magnetic splitting sextets at 77 K, rules out the presence of magnetic ordering as found for goethite[128] and akaganéite[129-131] above 77 K. Magnetic ordering in lepidocrocite,[132] ferrihydrite,[133,134] and ferritin[135,136] has only been observed in Mössbauer spectra recorded below 77 K, and is also dependent on sample preparation and morphology.

10　Therefore, the Fe K-edge XANES spectra of the iron loaded SECs formed from either FeCl$_3$ or FeCl$_2$ aqueous solutions and air dried indicate the presence of FeOOH, probably in a form more similar to ferrihydrite, which is less ordered, than goethite, akaganéite or lepidocrocite. Several workers have commented that identifying the various iron oxyhydroxides unambiguously is very difficult, if not impossible, using just the XANES spectra.[52,116,121]

15　In addition to the Fe K-edge XANES data, EXAFS data were also obtained for these samples, as well as the acetate standards, and it is illustrative to consider these first. Ferrous acetate is a 2D polymer with octahedral iron coordination with predominantly edge sharing of the octahedra, but with some vertex sharing resulting in three different iron sites. The structure contains a range of Fe-O distances (1.998 - 2.269 Å, $\bar{x}$ = 2.145 Å, σ_{n-1} = 0.083 Å) and Fe...Fe distances (3.2603 – 3.4288, $\bar{x}$ = 3.342 Å, σ_{n-1} = 0.075 Å).[99] Ferric acetate has a trimeric

20　structure with an oxygen atom at the centre of the planar Fe$_3$ triangle.[98] The octahedral iron atoms are surrounded by four equatorial oxygen atoms from the acetate groups (which bridge the iron atoms), one water and a slightly shorter bond to the oxygen in the centre of the cluster. In this case the spread of Fe-O distances is smaller (1.897 – 2.126 Å, $\bar{x}$ = 2.009 Å, σ_{n-1} = 0.061 Å) as is that of the Fe...Fe distances (3.2958 – 3.3017 Å, x = 3.299 Å, σ_{n-1} = 0.003 Å).[98] In contrast, cobalt acetate tetrahydrate is mononuclear with four equatorial water ligands and a pair of monodentate acetate ligands *trans* to each other with a much smaller distribution of Co-O distances (2.085 – 2.114 Å, x = 2.098 Å,

25　σ_{n-1} = 0.013 Å) and just one Co...Co at 4.774 Å.[137]

The fits to the EXAFS and Fourier transforms (FT) for these three samples are shown in Fig. 3 using the single crystal data as a starting point. The metal-oxygen shell is the first one in the FT and the effect of a decrease in the spread of Fe-O and Co-O distances can be seen as this peak in the FT gains intensity on going from ferrous acetate, to ferric acetate and finally cobalt acetate, and this is accompanied by

30　a reduction in the Debye-Waller factor in the refinements (Table 1). Whilst it was possible to model these data using more than one Fe-O or Co-O shell, this was not found to be statistically significant, and therefore in these and the following refinements the initial Fe-O shell was modelled using a single Fe-O distance. This allows for direct comparison of the Debye-Waller factors between the acetate and SEC spectra to examine the extent of disorder in the Fe-O distances in the SEC samples. The modelling produced high quality fits which are in good agreement with the published crystal structures for the mean Fe/Co-O and Fe...Fe and Co...Co distances in all three acetates. The

35　intensity of the more distant shell at *ca.* 4.5 Å in the ferrous acetate data is due to a multiple scattering interaction involving the iron, oxygen and methyl carbon of an acetate group. It should be noted that it is only possible to generate such high quality fits with a reasonably large number of shells, especially of the lighter atoms, by making recourse to the known structures.

Whilst the acetate data allow for comparison of Debye-Waller factors, the XANES data indicate that the structure is more similar to the

40　iron oxyhydroxides and oxides. Comparison of the Fe K-edge EXAFS data from the SECs in this work (Fig. 4), with the substantial previous reports on iron oxyhydroxides and oxides is made complicated by peak overlap as well as the use of different temperatures for the data collection. Data collected at cryogenic temperatures has enhanced intensity in the FT compared to that obtained at room temperature, and this tends to be more marked for second or third coordination shells. In general, the peaks due to Fe...Fe interactions at *ca.* 3 – 3.5 Å are more intense in the more ordered iron oxyhydroxide structures (goethite, akaganéite, lepidocrocite) than less ordered ones

45　(ferrihydrite, feroxyhte). The Fe K-edge EXAFS and FT data from the iron(III) loaded SEC samples shown in Fig. 4 are more similar to ferrihydrite[49,58,107,116,117,138-141] rather than goethite,[49,58,72,107,116,117,138,139,141,142] akaganéite,[141-144] or lepidocrocite.[107] The latter have higher intensity peaks in the FT arising from the Fe...Fe interactions compared with either 2 or 6 line ferrihydrite or feroxyhte. The intensity of the corner-sharing Fe...Fe interaction at ca 3.4 Å is lower in akaganéite than goethite,[142] and there are claims that FeOOH polymers have an akaganéite-like local structure.[142] The spectra of 1 line ferrihydrite, 2 line ferrihydrite and 3 line ferrihydrite are remarkably similar to

50　our data for the Fe^{III} SEC samples, although unfortunately, no detailed analysis was reported.[140] There is also a very good correspondence with the data from horse spleen ferritin and haemosiderin,[145] ferritin[103,136,146-148] and frataxin (yeast and human),[103] iron oxide nanoparticles formed by *Streptococcus suis*,[106,149] and iron in the basal ganglia of Parkinson's disease.[150]

The first peak in the FT of the Fe K-edge EXAFS data (Fig. 4) from the samples prepared using ferric chloride solution or ferrous chloride

55　solution and air dried could be fitted to a split first shell of 2 and 4 Fe-O interactions at 1.89(2) and 2.04(2) Å. However, as the split shell refinements are barely statistically significant, and the difference in the shells is only just resolvable using the Manceau and Drits test (k$_{max}$ ≥ π/2ΔR)[138] it was decided to use a single shell to allow comparison with the above acetate data. The single shell refinement gave a Fe-O distance of 2.01(2) Å for the FeCl$_3$ derived SEC sample. The Debye-Waller factor of 0.033 Å^2 is more similar to that of ferric acetate rather

ARTICLE TYPE

than ferrous acetate indicating a moderate, but not large spread of Fe-O distances. The second feature in the FT is made up of Fe...Fe interactions at 2.99(3), 3.42(3) and 3.67(4) Å with occupation numbers of 3, although the occupation numbers are not well defined. The more distant and relatively weak Fe...Fe interaction at 3.67(4) Å could also be fitted with a Fe...O distance at 3.5 Å. Whilst this was also observed for ferritin,[145] a Fe...Fe interaction makes more chemical sense in this case. The features at greater than 4 Å in the FT in Fig. 4(a)
[5] contain, in principle, additional information about the local iron environment. However, as they are relatively weak, and will be the result of a number of Fe...Fe interactions, some of which may involve multiple scattering, and there is little in the literature of pure phases to guide the analysis, it was not possible to obtain a meaningful fit to these features between 4 and 6 Å.

The Fe-O distances from the SECs of 2.01(2) Å (Table 2) are in good agreement with the ferric acetate data of 2.02(2) Å (Table 1) as well as work from both mineralogical and biological Fe^{III} samples including humic acid[151,152] and lignin.[153] Although Carta *et al*.[117] only
[10] observed a single Fe-O distance of 1.96 Å for 2 line and 6 line ferrihydrite nanoparticles, other workers have reported two Fe-O shells (1.95 and 2.09/2.10 Å) for ferrihydrite.[49,139] However, more recently Maillot *et al*. have interpreted Fe-O distances of 1.87 and 1.99 Å in their analysis of 2 line ferrihydrite and 1.88 and 2.00 Å in 6 line ferrihydrite as being indicative of ferrihydrite containing 20-30% of tetrahedral Fe^{III}.[141] This observation, together with the claim of Peak and Regier[154] that Fe L-edge XAS also supports the presence of tetrahedral Fe^{III} is controversial, and has not been universally accepted.[155-158] However, the models containing tetrahedral Fe^{III} agree with
[15] the controversial[159-162] ferrihydrite structure proposed by Michel.[163] The early Fe K-edge EXAFS work on ferritin identified a single Fe-O interaction at *ca*. 1.96 Å [102,146,147], although a more recent study found a split Fe-O first shell of 1.94 and 2.08 Å for human ferritin.[103] Therefore, the Fe-O distances within the SECs are entirely consistent with the presence of octahedral Fe^{III} coordinated to oxygen.

The Fe...Fe distances give valuable information about the ordering and association of the FeO_6 octahedra. Manceau and Drits carried out
[20] a very detailed investigation of the Fe...Fe interactions in the FeOOH family based on previous X-ray data, as well as their own Fe K-edge EXAFS data.[138] This revealed the following Fe...Fe interactions based on calculations from X-ray crystal structure data: goethite (α-FeOOH): 3.01 Å (edge sharing), 3.28 Å (edge sharing), 3.46 Å (double corner sharing); akaganéite (β-FeOOH): 3.03 Å, (edge sharing), 3.34 Å (edge sharing), 3.51 Å (double corner sharing); lepidocrocite (γ-FeOOH): 3.05, 3.06 Å (edge sharing), 3.87 Å (shared corner sharing).

[25]
Feroxyhyte and ferrihydrite structures were more complex and the increased distribution of Fe...Fe distances in the 3 Å shell was taken to indicate the presence of shorter Fe...Fe associated with face sharing. On this basis feroxyhyte has face and edge sharing (2.4 at 2.98 Å (average of 2.91 and 3.04)) and double corner sharing (2.7 at 3.41 Å) interactions; 6 line ferrihydrite has face and edge sharing (3 at 3.01 Å (average of 2.92 and 3.05)), and double corner sharing octahedra (6.5 at 3.44 Å). For 2 line ferrihydrite, the EXAFS and FTs were also
[30] dependent on the preparation method,[138] with the number of Fe...Fe interactions at 3.00 Å increasing compared to those at 3.44 Å, with longer ageing at 92° C. Work by Nichol *et al*. on the detailed analysis of FeOOH materials has found that Fe...Fe interactions of 2.95 Å are indicative of face sharing FeO_6 octahedra, 3.07 Å edge sharing and 3.44 Å double-corner sharing.[103] More recent work by Carta *et al*. observed Fe...Fe interactions at 2.87 (face sharing), 3.03 (edge sharing) and 3.45 Å (double corner sharing) for 2 and 6 line ferrihydrite.[117]

[35] It has been shown that Fe^{III} pre-cursors yield α- and β-FeOOH, whilst Fe^{II} oxidation goes to γ-FeOOH.[114] Hydrolysis of ferric chloride yields akaganéite (β-FeOOH)[164] and Fe K-edge EXAFS analysis indicated that partial hydrolysis of $FeCl_3$ solutions resulted in polymers with an akaganéite-like local structure (2.5 at 3.03 Å and 5.9 at 3.42 Å).[142] This is not that surprising, as whilst akaganéite is formally β-FeOOH, it has chloride in the solid state structure, but it is not directly associated with the iron.[165] Hydrolysis of ferric nitrate yields goethite.[142]

[40]
Our Fe...Fe distances of 2.99(3) and 3.42(3) Å in the SECs are in very good agreement with the values for both 2 line and 6 line ferrihydrite and indicate the presence of face, edge and double corner sharing octahedra. Therefore, both the XANES and EXAFS data are consistent with the presence of a disordered, or short range ordered, FeOOH material in the SEC samples derived from ferric chloride solutions.

[45] As noted previously, the Fe K-edge XANES spectra of the samples prepared from ferrous chloride solutions that had been air dried (see Fig. 2(c)) were essentially identical to those obtained when ferric chloride was used, indicating the presence of Fe^{III}. The Fe K-edge EXAFS and FTs for these samples are very similar to those prepared using $FeCl_3$ (Fig. 4). The Fe-O distance of 2.02(2) Å is essentially the same as for the ferric chloride derived sample, and the only significant difference in the fits is the slight elongation of the Fe...Fe distance from 2.99(3) to 3.06(3) Å, which was observed consistently between samples, and probably indicates a reduction in the number of face sharing
[50] interactions which are replaced by edge sharing. In addition, the Debye-Waller factor associated with the more distant shells have increased, indicating either greater disorder, or lower occupation numbers for the $FeCl_2$ derived samples, compared with the $FeCl_3$ derived samples. The lack of any weak features beyond 4 Å in the FT of these data is also indicative of shorter range order than observed in the $FeCl_3$ derived samples. It has been noted previously that Fe^{II} oxidation results in the γ-FeOOH (lepidocrocite) phase,[114] which has longer Fe...Fe

interactions than the other oxyhydroxy phases.

Therefore, the iron environment in the Fe^{III} samples derived from both routes appears to closely resemble that in ferrihydrite and by inference ferritin. Whilst the XANES spectra are essentially identical for the $FeCl_3$ and $FeCl_2$ derived samples, there is some indication of a slight elongation of the Fe...Fe interactions in the samples derived from ferrous chloride solutions indicating fewer face sharing interactions. It should be noted that the exact structure of ferrihydrite is still open to considerable debate and controversy, especially relating to the absence or presence of tetrahedral Fe^{3+} in the structure.[141,154-158,163,166-169]

When the Fe^{II} loaded sporopollenin samples were prepared in the absence of air (Schlenk techniques) using either $FeCl_2$ or $Fe(BF_4)_2$ solutions, the Fe K-edge XANES spectra (Fig. 2(d) and (f)) showed an edge shift to lower energy of *ca.* 2 eV compared to the Fe^{III} samples (Fig. 2(b) and (c)), which is about half that observed for the Fe^{III} and Fe^{II} acetates (Fig 2(a) and Fig (2g)). There was no significant change in the spectrum of a sample prepared anaerobically using $FeCl_2$ and stored under Ar (Fig. 2(d)) and one that had been stored under air for two weeks (Fig. 2(e)). The Fe K-edge XANES spectra of the samples prepared using $Fe(BF_4)_2$ solutions (Fig. 2(f)) were similar to those from $FeCl_2$, but there is a shoulder present just after the edge and the pre-edge features are less well defined. The edge positions of 7122.4 eV are intermediate to those of 7124.5 eV for ferric acetate (Fig. 2 (a)) and 7120.6 eV for ferrous acetate (Fig. 2(f)). As noted above, there is usually an edge shift of *ca.* 4 eV between Fe^{II} and Fe^{III} not only for coordination complexes but also for iron oxides,[72] iron sulfates,[100] wüstite to akaganéite,[101] and in fayalite[170] and ferrous hydroxychloride.[56] Whilst a shift of *ca.* 2 eV is observed between Fe_3O_4 and γ-Fe_2O_3[113,120,171] or Fe_3O_4 and α-Fe_2O_3,[72] the edge structure and the first derivatives of the spectra in Fig 2(d-f) indicate a single edge position, which is not observed in Fe_3O_4,[70,72,103] where both Fe^{II} and Fe^{III} are present. The pre-edge features are also intermediate between Fe^{II} and Fe^{III} and show more structure than those of the Fe^{III} loaded sporopollenin samples, but these have been shown previously to be less sensitive to oxidation state for oxide and oxyhydroxy minerals.[72] Although a 1.4 eV shift in position of the pre-edge features for pure Fe^{II} to Fe^{III} samples was observed, there is no simple linear relationship for mechanical mixtures of compounds.[100] Therefore, it appears from the XANES data that even with anaerobic preparation and handling there is a mixture of Fe^{II} and Fe^{III} formed between Fe^{II} pre-cursors and the SECs, and that there is little difference if the samples prepared using $FeCl_2$ are stored under Ar or air for two weeks.

The Fe K-edge EXAFS data from the samples prepared from $FeCl_2$ under anaerobic conditions were initially refined with the same model used for the Fe^{III} samples, but as is clear from the FTs, (Fig. 5) the peaks due to the more remote Fe...Fe shells are much less intense. Although a split Fe-O shell of 1.91(2) and 2.08(2) Å could be fitted to the data, this was barely statistically significant and a single Fe-O shell was used to remain consistency with the other data (Table 1 and 2) together with a split Fe...Fe, but with lower occupation numbers. The Fe-O distance of 2.06(2) Å for the sample prepared using $FeCl_2$ solutions and stored under argon was essentially identical to that for a $FeCl_2$ sample aged for 2 weeks in air (2.06(2) Å) and a sample prepared with $Fe(BF_4)_2$ solutions (2.05(2) Å), although the data for the latter one are relatively noisy (which is not unexpected given the lower iron loading). The Debye-Waller factors for these Fe-O interactions are closer to those observed for ferrous rather than ferric acetate and are larger than those for the Fe^{III}-O shells above, indicating a greater spread of Fe-O distances. There was no evidence for the presence of chloride in the first coordination shell, thus ruling out the formation of ferrous hydroxychloride.[56] The second much weaker feature in the FT was fitted to Fe...Fe interactions at 3.06(3) and 3.39(3) Å in the case of the $FeCl_2$ prepared materials. The first of these is very similar to that of the SECs containing oxidised Fe^{II}, although the second one is shorter than that observed in the Fe^{III} or Fe^{II} oxidised samples. These values are consistent with Fe...Fe edge and double corner sharing, but with less evidence for face sharing than above. For the $Fe(BF_4)_2$ derived SEC sample the Fe..Fe interactions were sufficiently weak (this may be caused by the relatively noisy data) as to make them almost below detection, although they are included in the fit (with large and poorly defined Debye-Waller factors) for consistency.

The intensity of the feature at 6.5 to 7.5 Å^{-1} in the Fe K-edge EXAFS spectra has been interpreted as a sensitive measure of the extent of Fe...Fe interaction,[102,149] and it is clear that in the EXAFS of the these samples (Fig. 5) this feature is much weaker than that of the Fe^{III} samples (Fig. 4), confirming a reduction in Fe...Fe interactions.

The Fe-O distances of 2.06(2) Å are slightly longer than those observed for the Fe^{III} SEC samples of 2.01(2) and 2.02(2) Å as might be expected for a reduction in oxidation state. The EXAFS analysis of the ferric and ferrous acetates gave Fe-O distances of 2.01(2) and 2.13(2) Å, respectively. X-ray diffraction data gives mean Fe-O distances of 2.157 and 2.179 Å for the two Fe^{II} octahedral iron sites in fayalite (Fe_2SiO_4) at room temperature.[172] In wüstite (FeO) the Fe-O octahedral distances of 2.14-2.16 Å [173,174] are similar to those in fayalite. In $[Fe(H_2O)_6]^{3+}(NO_3)_3.3H_2O$ the average Fe-O distance is 1.986(7) Å for the two octahedral sites compared to an average of 2.13 Å for $[Fe(H_2O)_6]^{2+}$.[175] In $[Fe(H_2O)_6]^{3+}(ClO_4)_3.3H_2O$ the Fe-O distance is 1.997 Å. [176] In magnetite the Fe-O distance associated with the octahedral sites (half Fe^{II} half Fe^{III}) is 2.046 Å whereas the Fe-O distance for tetrahedral Fe^{III} is 1.910 Å.[177]

Therefore, the Fe-O distances in the SECs reacted with Fe^{II} salts under anaerobic conditions are not characteristic of pure Fe^{II}-O interactions, but indicate that there is a mixture of Fe^{II} and Fe^{III} present, in agreement with the XANES data. The much weaker Fe...Fe interactions at 3.06(3) and 3.39(3) Å are similar to those observed for the Fe^{III} samples, but the first one is at a slightly longer distance indicating a lower extent of face sharing compared to edge sharing of the octahedra. The lower intensity of these peaks could be due to both lower occupation numbers and higher disorder of the Fe-Fe distances, both of which indicate either smaller particles (higher surface

ARTICLE TYPE

area) or more disorder of larger particles. This behaviour has been observed previously for mesoporous α-Fe$_2$O$_3$ with disordered walls, where the intensity of the Fe...Fe interaction was much reduced compared to mesoporous α-Fe$_2$O$_3$ with ordered walls or bulk α-Fe$_2$O$_3$.[178] However, as both the Fe K-edge XANES and EXAFS data indicate a mixture of Fe^{II} and Fe^{III} in these SEC samples a much more probable scenario is that there is a mixture of the ferrihydrite-like Fe^{III} material, together with a Fe^{II} phase involving interaction with the carboxylate

5 and phenolate groups on the SEC surface that will have much reduced Fe...Fe interactions. It should be noted that there are subtle differences between the spectra of the anaerobically prepared FeCl$_2$ and Fe(BF$_4$)$_2$ samples.

Micro-focus Fe Kα XRF imaging and XANES spectroscopy

Whilst it is clear is that the iron-iron interactions are much more significant in the samples containing all Fe^{III} (either prepared from ferric

10 chloride or from ferrous chloride and allowed to oxidise) than those containing a higher proportion of Fe^{II}, the XANES and EXAFS data do not explain why the iron loading is so much higher in the samples prepared from ferrous chloride rather than ferric chloride solutions. To gain insight into the spatial distribution of iron a micro-focus XRF study was carried out.

Fig. 6 shows the Fe Kα XRF image of the SECs prepared from a ferric chloride aqueous solution and with air drying. (The optical and X-

15 ray images do not superimpose due to the different collection geometries with the optical image collected at 45° to the incident X-ray beam, whereas the XRF image is collected at 90° [86]) Whilst there is some evidence for the iron being associated with the SEC structure at both the 5 and 1 μm pixel level, the correlation is really quite poor. However, the Fe K-edge XANES spectra recorded for individual SECs (not shown) were identical to those in Fig. 2(b) and are consistent with the presence of Fe^{III}. Fig. 7 shows the Fe Kα X-ray imaging results for SECs reacted with aqueous FeCl$_2$ solutions, and air dried. The Fe Kα XRF image clearly shows that the iron is very closely associated with

20 the structure of both the cap and trilete areas of the SECs as in Fig. 1. The Fe K-edge XANES spectra recorded from a single SEC are essentially identical to that in Fig. 2(c) indicating that the spectra from the bulk samples are consistent with those from single SECs, and in this case confirms the presence of Fe^{III} rather than Fe^{II}. When the Fe Kα XRF experiment was repeated with SECs prepared from aqueous FeCl$_2$ solutions under anaerobic preparation and handling conditions, the Fe Kα XRF image (Fig. 7) was very similar to that observed in Fig. 6, again with the iron clearly associated with the SEC structure. However, in this case the Fe K-edge XANES spectrum from a single

25 SEC was different with an edge position of 7122.4 eV very similar to that observed for the bulk in Fig. 2(d).

Therefore, the Fe Kα XRF images indicate that the interaction of the iron with the SEC is very dependent on whether Fe^{II} or Fe^{III} is used as the starting material. In the case of the ferric solutions, it appears that hydrolysis results in the formation of an oxyhydroxy species, which then coats the surface of the SEC. For the samples prepared from ferrous solutions, there appears to be a much more specific interaction

30 between the iron and the SEC surface, and that on oxidation the structure of the oxyhydroxy phase is similar, but not identical to that observed from ferric solutions. The exines appear to remain hollow from both the SEM and XRF images.

Conclusions

The use of X-ray absorption spectroscopy has given unique insights into the structure-property relationships of the Fe-SEC conjugates which will provide the foundation for further studies, including detailed Mössbauer experiments. The bulk Fe K-edge XANES and EXAFS

35 data for the SECs prepared using either ferric or ferrous chloride solutions and air dried, indicate the presence of Fe^{III} in a ferrihydrite-like form, similar to that observed for ferritin. In contrast, when anaerobic techniques are employed, the Fe K-edge XANES and EXAFS spectra reveal the presence of a mixture of Fe^{III} and Fe^{II} environments. This is a surprising observation given the known anti-oxidant properties of sporopollenin.[79,82] However, the anti-oxidant properties may not be able to compensate for the high surface area of the SECs making oxidation facile when the samples are air dried. It has also been proposed that there is rapid electron transfer over the sporopollenin

40 surface,[79] which may also contribute to this redox chemistry.

The Fe Kα XRF images indicate that the interaction between iron and the SEC is different for Fe^{II} and Fe^{III} pre-cursors, with a much higher correlation between SEC structure and iron location for Fe^{II} than Fe^{III}. For the samples prepared from Fe^{III} it appears that the SEC is just covered/coated in the FeOOH material. In contrast, when FeCl$_2$ or Fe(BF$_4$)$_2$ solutions are used, there are specific interactions with the SEC

45 surface groups, potentially including the interior as well as the exterior, although it should be noted that the SECs remain hollow. These observations help to explain the much higher loadings of iron that are observed for samples prepared from aqueous solutions of FeCl$_2$ (routinely 30 mg g^{-1} and up to 40 mg g^{-1}), whereas values of only around a tenth of this are observed for samples prepared from aqueous solutions of FeCl$_3$. Therefore, both the initial iron oxidation state, and the subsequent processing, have a significant effect on the structure, and hence properties of the Fe-SEC conjugates.

50

There have been numerous investigations of the aqueous chemistry of Fe^{III} spanning coordination chemistry, environmental and geological chemistry, archaeological artefacts[56-58,124] and even the identification of akaganéite (impurities) formed in the presence of chloride during lunar missions.[179] What is clear is that iron hydrolysis chemistry is very complex, and in places controversial and contentious, and that the products formed are highly dependent on conditions.[180,181] For example Fe^{III} pre-cursors yield α- and β-FeOOH, whilst Fe^{II} oxidation goes to γ-FeOOH.[114] Hydrolysis of ferric nitrate yields goethite whilst hydrolysis of ferric chloride yields akaganéite (β-FeOOH).[164] This is not that surprising, as whilst akaganéite is formally β-FeOOH, it has chloride in the solid state structure, but it is not associated with the iron.[165] The fact that the XANES and EXAFS data of the sample prepared from $Fe(BF_4)_2$ solutions are subtly different from those using $FeCl_2$ solutions might indicate that an akaganéite-like phase plays an important role in the processes.

Acknowledgements

Notes and references

a Department of Chemistry, The University of Hull, Kingston upon Hull, HU6 7RX, U.K. Fax: 44 1482 466410; Tel: 44 1482 465442; E-mail: n.a.young@hull.ac.uk

b Hull York Medical School, The University of Hull, Kingston upon Hull HU6 7RX, U.K.

c Sporomex Ltd., Newland Avenue, Driffield, YO25 6TX, U.K.

d DUBBLE@ESRF, BP 220 Grenoble 38143, France

e Diamond Light Source, Harwell Science and Innovation Campus, Didcot, OX11 0DE, U.K.

f Department of Physics, University of Liverpool, L69 7ZE, U.K.

1. D. Tarn, C. E. Ashley, M. Xue, E. C. Carnes, J. I. Zink and C. J. Brinker, *Acc. Chem. Res.*, 2013, **46**, 792-801.

2. P. Tanner, P. Baumann, R. Enea, O. Onaca, C. Palivan and W. Meier, *Acc. Chem. Res.*, 2011, **44**, 1039-1049.

3. S. F. M. van Dongen, H.-P. M. de Hoog, R. J. R. W. Peters, M. Nallani, R. J. M. Nolte and J. C. M. van Hest, *Chem. Rev.*, 2009, **109**, 6212-6274.

4. S. Rieth, K. Hermann, B.-Y. Wang and J. D. Badjić, *Chem. Soc. Rev.*, 2011, **40**, 1609-1622.

5. C.-S. Ha and J. A. Gardella, *Chem. Rev.*, 2005, **105**, 4205-4232.

6. S. L. Atkin, S. Barrier, Z. Cui, P. D. I. Fletcher, G. Mackenzie, V. Panel, V. Sol and X. Zhang, *J. Photochem. Photobiol. B-Biol.*, 2011, **102**, 209-217.

7. J. Brooks and G. Shaw, *Chem. Geol.*, 1972, **10**, 69-87.

8. A. Diego-Taboada, L. Maillet, J. H. Banoub, M. Lorch, A. S. Rigby, A. N. Boa, S. L. Atkin and G. Mackenzie, *J. Mat. Chem. B*, 2013, **1**, 707-713.

9. A. Wakil, G. Mackenzie, A. Diego-Taboada, J. G. Bell and S. L. Atkin, *Lipids*, 2010, **45**, 645-649.

10. M. Lorch, M. J. Thomasson, A. Diego-Taboada, S. Barrier, S. L. Atkin, G. Mackenzie and S. J. Archibald, *Chem. Commun.*, 2009, 6442-6444.

11. G. Mackenzie and G. Shaw, *Int. J. Pept. Protein Res.*, 1980, **15**, 298-300.

12. R. Adamson, S. Gregson and G. Shaw, *Int. J. Pept. Protein Res.*, 1983, **22**, 560-564.

13. V. N. Paunov, G. Mackenzie and S. D. Stoyanov, *J. Mater. Chem.*, 2007, **17**, 609-612.

14. M. Keleş, *Synth. React. Inorg. Met.-Org. Nano-Metal Chem.*, 2013, **43**, 575-579.

15. G. Shaw, M. Sykes, R. W. Humble, G. Mackenzie, D. Marsden and E. Pehlivan, *Reactive Polymers*, 1988, **9**, 211-217.

16. M. Ersoz, S. Yildiz and E. Pehlivan, in *Ion Exchange Processes : Advances and Applications*, 1993, vol. 122, pp. 305-313.

17. E. Pehlivan and S. Yildiz, *Sep. Sci. Technol.*, 1994, **29**, 887-895.

18. M. Ersoz, E. Pehlivan, H. J. Duncan, S. Yildiz and M. Pehlivan, *Reactive Polymers*, 1995, **24**, 195-202.

19. A. Ayar, S. Yildiz and E. Pehlivan, *Sep. Sci. Technol.*, 1995, **30**, 3081-3086.

20. U. S. Vural, M. Ersoz and E. Pehlivan, *J. Appl. Polym. Sci.*, 1995, **58**, 2423-2428.

21. E. Pehlivan, U. S. Vural, A. Ayar and S. Yildiz, *Sep. Sci. Technol.*, 1996, **31**, 1643-1648.

22. M. Ersoz, Y. Cengeloglu, N. Gokdemir and M. Lale, *New J. Chem.*, 1997, **21**, 1067-1072.

23. M. Ersoz, M. Yigitoglu and A. Ayar, *J. Appl. Polym. Sci.*, 1997, **64**, 1225-1234.

24. A. Ayar, A. I. Pekacar and B. Mercimek, *Colloid Surf. A-Physicochem. Eng. Asp.*, 2003, **212**, 51-55.

25. M. Uçan, A. Gürten and A. Ayar, *Colloid Surf. A-Physicochem. Eng. Asp.*, 2003, **219**, 193-199.

26. A. Ayar and A. A. Gürten, *Colloid Surf. A-Physicochem. Eng. Asp.*, 2003, **229**, 149-155.

27. N. Erciyes, A. A. Gürten, M. I. Abdullah and A. Ayar, *J. Colloid Interface Sci.*, 2004, **278**, 91-95.

28. A. Ayar and B. Mercimek, *Process Biochem.*, 2006, **41**, 1553-1559.

29. A. Ayar, S. Gürsal, A. A. Gürten and O. Gezici, *Desalination*, 2008, **219**, 160-170.

30. T. Gürten and O. Serindag, *Acta Phys.-Chim. Sin.*, 2009, **25**, 2218-2224.

31. N. Unlu and M. Ersoz, *J. Hazard. Mater.*, 2006, **136**, 272-280.

32. M. Arslan, Z. Temocin and M. Yigitoglu, *Fresenius Environ. Bull.*, 2004, **13**, 616-619.

33. E. Pehlivan, M. Ersoz, M. Pehlivan, S. Yildiz and H. J. Duncan, *J. Colloid Interface Sci.*, 1995, **170**, 320-325.

ARTICLE TYPE

34. N. Unlu and M. Ersoz, *Sep. Purif. Technol.*, 2007, **52**, 461-469.

35. İ. H. Gübbük, *J. Hazard. Mater.*, 2011, **186**, 416-422.

36. A. Çimen, A. Bilgiç, A. N. Kursunlu, İ. H. Gübbük and H. İ. Uçan, *Desalin. Water Treat.*, 2013, 1-11.

37. N. Kocak, M. Sahin and İ. H. Gübbük, *J. Inorg. Organomet. Polym. Mater.*, 2012, **22**, 852-859.

38. M. Sahin, İ. H. Gübbük and N. Kocak, *J. Inorg. Organomet. Polym. Mater.*, 2012, **22**, 1279-1286.

39. F. Gode and E. Pehlivan, *Bioresour. Technol.*, 2007, **98**, 904-911.

40. S. Sayin, İ. H. Gübbük and M. Yilmaz, *J. Incl. Phenom. Macrocycl. Chem.*, 2013, **75**, 111-118.

41. S. Kucukkolbasi, Z. Ö. Erdoğan, N. Kocak, M. Sahin and İ. H. Gübbük, *Water Air Soil Pollut.*, 2013, **224**, 1474.

42. İ. H. Gübbük, L. Gürfidan, S. Erdemir and M. Yilmaz, *Water Air Soil Pollut.*, 2012, **223**, 2623-2632.

43. M. A. Kamboh and M. Yilmaz, *Desalination*, 2013, **310**, 67-74.

44. B. J. R. Thio, K. K. Clark and A. A. Keller, *J. Hazard. Mater.*, 2011, **194**, 53-61.

45. E. Yilmaz, M. Sezgin and M. Yilmaz, *J. Mol. Catal. B-Enzym.*, 2010, **62**, 162-168.

46. E. Yilmaz, M. Sezgin and M. Yilmaz, *J. Mol. Catal. B-Enzym.*, 2011, **69**, 35-41.

47. M. Bonnin-Mosbah, A. S. Simionovici, N. Métrich, J.-P. Duraud, D. Massare and P. Dillmann, *J. Non-Cryst. Solids*, 2001, **288**, 103-113.

48. M. Bonnin-Mosbah, N. Métrich, J. Susini, M. Salomé, D. Massare and B. Menez, *Spectrochimica Acta Part B-Atomic Spectroscopy*, 2002, **57**, 711-725.

49. B. M. Toner, C. M. Santelli, M. A. Marcus, R. Wirth, C. S. Chan, T. McCollom, W. Bach and K. J. Edwards, *Geochim. Cosmochim. Acta*, 2009, **73**, 388-403.

50. L. E. Mayhew, S. M. Webb and A. S. Templeton, *Environ. Sci. Technol.*, 2011, **45**, 4468-4474.

51. M. Terabayashi, T. Matsui, K. Okamoto, H. Ozawa, Y. Kaneko and S. Maruyama, *Isl. Arc.*, 2013, **22**, 37-50.

52. J. Prietzel, J. Thieme, K. Eusterhues and D. Eichert, *Eur. J. Soil Sci.*, 2007, **58**, 1027-1041.

53. K. Wovkulich, B. J. Mailloux, B. C. Bostick, H. L. Dong, M. E. Bishop and S. N. Chillrud, *Geochim. Cosmochim. Acta*, 2012, **91**, 254-270.

54. S. Réguer, P. Dillmann, F. Mirambet and L. Bellot-Gurlet, *Nucl. Instrumen. Meth. B*, 2005, **240**, 500-504.

55. S. Réguer, P. Dillmann, F. Mirambet, J. Susini and P. Lagarde, *Appl. Phys. A*, 2006, **83**, 189-193.

56. S. Réguer, P. Dillmann and F. Mirambet, *Corros. Sci.*, 2007, **49**, 2726-2744.

57. J. Monnier, D. Neff, S. Réguer, P. Dillmann, L. Bellot-Gurlet, E. Leroy, E. Foy, L. Legrand and I. Guillot, *Corros. Sci.*, 2010, **52**, 695-710.

58. J. Monnier, S. Réguer, D. Vantelon, P. Dillmann, D. Neff and I. Guillot, *Appl. Phys. A*, 2010, **99**, 399-406.

59. J. Monnier, D. Vantelon, S. Réguer and P. Dillmann, *Actual. Chim.*, 2011, **356-57**, 109-112.

60. A. Mikhaylova, M. Davidson, H. Toastmann, J. E. T. Channell, Y. Guyodo, C. Batich and J. Dobson, *J. R. Soc. Interface*, 2005, **2**, 33-37.

61. J. F. Collingwood, A. Mikhaylova, M. R. Davidson, C. Batich, W. J. Streit, T. Eskin, J. Terry, R. Barrea, R. S. Underhill and J. Dobson, in *Fifth International Conference on Fine Particle Magnetism. J. Phys. Conf. Ser.*, ed. Q. Pankhurst, 2005, vol. 17, pp. 54-60.

62. J. F. Collingwood, A. Mikhaylova, M. Davidson, C. Batich, W. J. Streit, J. Terry and J. Dobson, *J. Alzheimers Dis.*, 2005, **7**, 267-272.

63. J. Collingwood and J. Dobson, *J. Alzheimers Dis.*, 2006, **10**, 215-222.

64. A. E. Oakley, J. F. Collingwood, J. Dobson, G. Love, H. R. Perrott, J. A. Edwardson, M. Elstner and C. M. Morris, *Neurology*, 2007, **68**, 1820-1825.

65. J. F. Collingwood, R. K. K. Chong, T. Kasama, L. Cervera-Gontard, R. E. Dunin-Borkowski, G. Perry, M. Pósfai, S. L. Siedlak, E. T. Simpson, M. A. Smith and J. Dobson, *J. Alzheimers Dis.*, 2008, **14**, 235-245.

66. J. F. Collingwood, M. R. Davidson, S. Chandra, A. Mikhaylova, J. Terry, C. Batich, P. Quinn, J. Forder, C. M. Morris and J. Dobson, *Mov. Disord.*, 2008, **23**, 182.

67. C. Exley, E. House, J. F. Collingwood, M. R. Davidson, D. Cannon and A. M. Donald, *J. Alzheimers Dis.*, 2010, **20**, 1159-1165.

68. J. J. Gallagher, M. E. Finnegan, B. Grehan, J. Dobson, J. F. Collingwood and M. A. Lynch, *J. Alzheimers Dis.*, 2012, **28**, 147-161.

69. A. J. Westphal, S. C. Fakra, Z. Gainsforth, M. A. Marcus, R. C. Ogliore and A. L. Butterworth, *ApJ*, 2009, **694**, 18-28.

70. J. C. Bridges, M. J. Burchell, H. C. Changela, N. J. Foster, J. A. Creighton, J. D. Carpenter, S. J. Gurman, I. A. Franchi and H. Busemann, *Meteorit. Planet. Sci*, 2010, **45**, 55-72.

71. R. C. Ogliore, A. L. Butterworth, S. C. Fakra, Z. Gainsforth, M. A. Marcus and A. J. Westphal, *Earth Planet. Sci. Lett.*, 2010, **296**, 278-286.

72. H. G. Changela, J. C. Bridges and S. J. Gurman, *Geochim. Cosmochim. Acta*, 2012, **98**, 282-294.

73. S. Bernard, K. Benzerara, O. Beyssac, G. E. Brown, L. G. Stamm and P. Duringer, *Rev. Palaeobot. Palynology*, 2009, **156**, 248-261.

74. A. Diego-Taboada, P. Cousson, E. Raynaud, Y. K. Huang, M. Lorch, B. P. Binks, Y. Queneau, A. N. Boa, S. L. Atkin, S. T. Beckett and G. Mackenzie, *J. Mater. Chem.*, 2012, **22**, 9767-9773.

75. S. Barrier, A. Diego-Taboada, M. J. Thomasson, L. Madden, J. C. Pointon, J. D. Wadhawan, S. T. Beckett, S. L. Atkin and G. Mackenzie, *J. Mater. Chem.*, 2011, **21**, 975-981.

76. S. Barrier, A. S. Rigby, A. Diego-Taboada, M. J. Thomasson, G. Mackenzie and S. L. Atkin, *LWT-Food Sci. Technol.*, 2010, **43**, 73-76.

77. S. L. Atkin, S. Barrier, S. T. Beckett, T. Brown, G. Mackenzie and L. Madden, in *Chemistry of Nucleic Acid Components*, 2005, vol. 7, pp. 307-311.

78. B. P. Binks, A. N. Boa, M. A. Kibble, G. Mackenzie and A. Rocher, *Soft Matter*, 2011, **7**, 4017-4024.

79. M. J. Thomasson, D. J. Baldwin, A. Diego-Taboada, S. L. Atkin, G. Mackenzie and J. D. Wadhawan, *Electrochem. Commun.*, 2010, **12**, 1428-1431.

80. S. Barrier, A. Löbbert, A. J. Boasman, A. N. Boa, M. Lorch, S. L. Atkin and G. Mackenzie, *Green Chem.*, 2010, **12**, 234-240.

81. B. P. Binks, J. H. Clint, G. Mackenzie, C. Simcock and C. P. Whitby, *Langmuir*, 2005, **21**, 8161-8167.

82. I. Orhan, B. Özçelik, S. Aslan, M. Kartal, T. Karaoglu, B. Şener, S. Terzioglu and M. I. Choudhary, *Phytochem Rev*, 2007, **6**, 189-196.

83. *Nutrition for Health and Development: A global agenda for combating malnutrition*, World Health Organization, Geneva, 2000.

84. M. Coplin, S. Schuette, G. Leichtmann and B. Lashner, *Clin. Ther.*, 1991, **13**, 606-612.

85. S. Nikitenko, A. M. Beale, A. M. J. van der Eerden, S. D. M. Jacques, O. Leynaud, M. G. O'Brien, D. Detollenaere, R. Kaptein, B. M. Weckhuysen and W. Bras, *J. Synchrotron Rad.*, 2008, **15**, 632-640.

86. J. F. W. Mosselmans, P. D. Quinn, A. J. Dent, S. A. Cavill, S. D. Moreno, A. Peach, P. J. Leicester, S. J. Keylock, S. R. Gregory, K. D. Atkinson and J. R. Rosell, *J. Synchrotron Rad.*, 2009, **16**, 818-824.

87. A. C. Thompson, D. Vaughan, D. T. Attwood, E. M. Gullikson, M. R. Howells, J. B. Kortright, A. L. Robinson, J. H. Underwood, K. J. Kim, J. Kirz, I. Lindau, P. Pianetta, H. Winick, G. P. Williams and J. H. Scofield, *Center for X-ray Optics and Advanced Light Source X-ray Data Booklet*, 2nd edn., Lawrence Berkeley National Laboratory, University of California, Berkeley, California, USA, 2001.

88. B. Ravel and M. Newville, *J. Synchrotron Rad.*, 2005, **12**, 537-541.

89. N. Binsted, *PAXAS, Program for the analysis of X-ray absorption spectra*, (1988) University of Southampton, U.K.

90. A. Tenderholt, B. Hedman and K. O. Hodgson, *AIP Conf. Proc.*, 2007, **882**, 105-107.

91. N. Binsted, *EXCURV98, CCLRC Daresbury Laboratory Computer Program*, (1998) CCLRC, Daresbury Laboratory, U.K.

92. V. A. Solé, E. Papillon, M. Cotte, P. Walter and J. Susini, *Spectrochim. Acta B*, 2007, **62**, 63-68.

93. W. Punt, P. P. Hoen, S. Blackmore, S. Nilsson and A. Le Thomas, *Rev. Palaeobot. Palynology*, 2007, **143**, 1-81.

94. J. R. Rowley, J. J. Skvarla and G. El-Ghazaly, *Can. J. Bot. Rev. Can.Bot.*, 2003, **81**, 1070-1082.

95. T. E. Westre, P. Kennepohl, J. G. De Witt, B. Hedman, K. O. Hodgson and E. I. Solomon, *J. Am. Chem. Soc.*, 1997, **119**, 6297-6314.

96. B. N. Figgis and G. B. Robertson, *Nature*, 1965, **205**, 694-695.

97. K. I. Turte, S. G. Shova, V. M. Meriacre, M. Gdaniec, Y. A. Simonov, J. Lipkowski, J. Bartolome, F. Wagner and G. Filoti, *J. Struct. Chem.*, 2002, **43**, 108-117.

98. S. Yao, J. Liu and Q. Han, *Acta Cryst. E*, 2008, **64**, m989.

99. B. Weber, R. Betz, W. Bauer and S. Schlamp, *Z. Anorg. Allg. Chem.*, 2011, **637**, 102-107.

100. M. Wilke, F. Farges, P. E. Petit, G. E. Brown and F. Martin, *Am. Mineral.*, 2001, **86**, 714-730.

101. K. S. Lin, Z. P. Wang, S. Chowdhury and A. K. Adhikari, *Thin Solid Films*, 2009, **517**, 5192-5196.

102. G. S. Waldo, E. Wright, Z. H. Whang, J. F. Briat, E. C. Theil and D. E. Sayers, *Plant Physiol.*, 1995, **109**, 797-802.

103. H. Nichol, O. Gakh, H. A. O'Neill, I. J. Pickering, G. Isaya and G. N. George, *Biochemistry*, 2003, **42**, 5971-5976.

104. B. F. G. Popescu, I. J. Pickering, G. N. George and H. Nichol, *J. Inorg. Biochem.*, 2007, **101**, 957-966.

105. N. Gálvez, B. Fernández, P. Sánchez, R. Cuesta, M. Ceolín, M. Clemente-León, S. Trasobares, M. López-Haro, J. J. Calvino, O. Stéphan and J. M. Domínguez-Vera, *J. Am. Chem. Soc.*, 2008, **130**, 8062-8068.

106. T. Haikarainen, P. Paturi, J. Lindén, S. Haataja, W. Meyer-Klaucke, J. Finne and A. C. Papageorgiou, *J. Biol. Inorg. Chem.*, 2011, **16**, 799-807.

107. A. G. Gault, A. Ibrahim, S. Langley, R. Renaud, Y. Takahashi, C. Boothman, J. R. Lloyd, I. D. Clark, F. G. Ferris and D. Fortin, *Chem. Geol.*, 2011, **281**, 41-51.

108. A. K. Powell, in *Metal Ions in Biological Systems*, eds. A. Sigel and H. Sigel, Marcel Dekker, New York, 1998, vol. 35: Iron Transport and Storage Microorganisms, Plants, and Animals, pp. 515-561.

109. N. E. Le Brun, A. Crow, M. E. P. Murphy, A. G. Mauk and G. R. Moore, *Biochim. Biophys. Acta*, 2010, **1800**, 732-744.

110. F. M. Michel, H.-A. Hosein, D. B. Hausner, S. Debnath, J. B. Parise and D. R. Strongin, *Biochim. Biophys. Acta*, 2010, **1800**, 871-885.

111. E. C. Theil, R. K. Behera and T. Tosha, *Coord. Chem. Rev.*, 2013, **257**, 579-586.

112. J. H. Jung, T. W. Eom, Y. P. Lee, J. Y. Rhee and E. H. Choi, *J. Magn. Magn. Mater.*, 2011, **323**, 3077-3080.

113. H. Okudera, A. Yoshiasa, K. Murai, M. Okube, T. Takeda and S. Kikkawa, *J. Mineral. Petrol. Sci.*, 2012, **107**, 127-132.

114. J. M. Combes, A. Manceau, G. Calas and J. Y. Bottero, *Geochim. Cosmochim. Acta*, 1989, **53**, 583-594.

115. L. X. Chen, T. Liu, M. C. Thurnauer, R. Csencsits and T. Rajh, *J. Phys. Chem. B*, 2002, **106**, 8539-8546.

116. P. A. O'Day, N. Rivera, R. Root and S. A. Carroll, *Am. Mineral.*, 2004, **89**, 572-585.

117. D. Carta, M. F. Casula, A. Corrias, A. Falqui, G. Navarra and G. Pinna, *Mater. Chem. Phys.*, 2009, **113**, 349-355.

118. S. Das, M. J. Hendry and J. Essilfie-Dughan, *Environ. Sci. Technol.*, 2011, **45**, 268-275.

119. L. C. C. Ferraz, W. M. Carvalho, D. Criado and F. L. Souza, *ACS Appl. Mater. Interfaces*, 2012, **4**, 5515-5523.

120. L. J. Oblonsky, M. P. Ryan and H. S. Isaacs, *Corros. Sci.*, 2000, **42**, 229-241.

121. T. Rennert, K. Eusterhues, V. De Andrade and K. U. Totsche, *Chem. Geol.*, 2012, **332**, 116-123.

122. H. Konishi, M. Yamashita, H. Uchida and J. Mizuki, *Mater. Trans.*, 2005, **46**, 329-336.

123. J. M. Combes, A. Manceau and G. Calas, *Geochim. Cosmochim. Acta*, 1990, **54**, 1083-1091.

ARTICLE TYPE

124. J. Monnier, L. Legrand, L. Bellot-Gurlet, E. Foy, S. Réguer, E. Rocca, P. Dillmann, D. Neff, F. Mirambet, S. Perrin and I. Guillot, *J. Nucl. Mater.*, 2008, **379**, 105-111.

125. T. Mathew, K. Suzuki, Y. Ikuta, Y. Nagai, N. Takahashi and H. Shinjoh, *Angew. Chem. Int. Ed.*, 2011, **50**, 7381-7384.

126. T. Mathew, K. Suzuki, Y. Nagai, T. Nonaka, Y. Ikuta, N. Takahashi, N. Suzuki and H. Shinjoh, *Chem. Eur. J.*, 2011, **17**, 1092-1095.

127. F. Glover, K. L. Whitworth, P. Kappen, D. S. Baldwin, G. N. Rees, J. A. Webb and E. Silvester, *Environ. Sci. Technol.*, 2011, **45**, 2591-2597.

128. C. A. Barrero and K. E. García, *J. Chem. Phys.*, 2013, **139**, 034703.

129. E. Murad, *Clay Minerals*, 1979, **14**, 273-283.

130. S. Musić, G. P. Santana, G. Šmit and V. K. Garg, *J. Alloys Compd.*, 1998, **278**, 291-301.

131. C. A. Barrero, K. E. García, A. L. Morales, S. Kodjikian and J. M. Greneche, *J. Phys. Conds. Mat.*, 2006, **18**, 6827-6840.

132. E. Murad and U. Schwertmann, *Mineral. Mag.*, 1984, **48**, 507-511.

133. E. Murad and U. Schwertmann, *Am. Mineral.*, 1980, **65**, 1044-1049.

134. R. K. Kukkadapu, J. M. Zachara, J. K. Fredrickson, S. C. Smith, A. C. Dohnalkova and C. K. Russell, *Am. Mineral.*, 2003, **88**, 1903-1914.

135. J. Webb, T. G. St. Pierre, K. C. Tran, W. Chua-anusorn, D. J. Macey and P. Pootrakul, *Inorg. Chim. Acta*, 1996, **243**, 121-125.

136. T. G. St. Pierre, P. Chan, K. R. Bauchspiess, J. Webb, S. Betteridge, S. Walton and D. P. E. Dickson, *Coord. Chem. Rev.*, 1996, **151**, 125-143.

137. A. N. Sobolev, E. B. Miminoshvili, K. E. Miminoshvili and T. N. Sakvarelidze, *Acta Cryst. E*, 2003, **59**, m836-m837.

138. A. Manceau and V. A. Drits, *Clay Minerals*, 1993, **28**, 165-184.

139. G. A. Waychunas, C. S. Kim and J. F. Banfield, *J. Nanopart. Res.*, 2005, **7**, 409-433.

140. H. Liu, Y. Wang, Y. Ma, Y. Wei and G. Q. Pan, *Chemosphere*, 2010, **79**, 802-806.

141. F. Maillot, G. Morin, Y. H. Wang, D. Bonnin, P. Ildefonse, C. Chaneac and G. Calas, *Geochim. Cosmochim. Acta*, 2011, **75**, 2708-2720.

142. J. Y. Bottero, A. Manceau, F. Villieras and D. Tchoubar, *Langmuir*, 1994, **10**, 316-319.

143. T. Ishikawa, T. Motoki, R. Katoh, A. Yasukawa, K. Kandori, T. Nakayama and F. Yuse, *J. Colloid Interface Sci.*, 2002, **250**, 74-81.

144. T. Ishikawa, R. Katoh, A. Yasukawa, K. Kandori, T. Nakayama and F. Yuse, *Corros. Sci.*, 2001, **43**, 1727-1738.

145. P. Mackle, C. D. Garner, R. J. Ward and T. J. Peters, *Biochim. Biophys. Acta*, 1991, **1115**, 145-150.

146. S. M. Heald, E. A. Stern, B. Bunker, E. M. Holt and S. L. Holt, *J. Am. Chem. Soc.*, 1979, **101**, 67-73.

147. S. L. Heath, J. M. Charnock, C. D. Garner and A. K. Powell, *Chem. Eur. J.*, 1996, **2**, 634-639.

148. L. Toussaint, M. G. Cuypers, L. Bertrand, L. Hue, C. V. Romão, L. M. Saraiva, M. Teixeira, W. Meyer-Klaucke, M. C. Feiters and R. R. Crichton, *J. Biol. Inorg. Chem.*, 2009, **14**, 35-49.

149. A. Kauko, A. T. Pulliainen, S. Haataja, W. Meyer-Klaucke, J. Finne and A. C. Papageorgiou, *J. Mol. Biol.*, 2006, **364**, 97-109.

150. P. D. Griffiths, B. R. Dobson, G. R. Jones and D. T. Clarke, *Brain*, 1999, **122**, 667-673.

151. G. Davies, A. Fataftah, A. Cherkasskiy, E. A. Ghabbour, A. Radwan, S. A. Jansen, S. Kolla, M. D. Paciolla, L. T. Sein, W. Buermann, M. Balasubramanian, J. Budnick and B. Xing, *J. Chem. Soc., Dalton Trans.*, 1997, 4047-4060.

152. T. Karlsson and P. Persson, *Geochim. Cosmochim. Acta*, 2010, **74**, 30-40.

153. E. Guillon, P. Merdy and M. Aplincourt, *Chem. Eur. J.*, 2003, **9**, 4479-4484.

154. D. Peak and T. Regier, *Environ. Sci. Technol.*, 2012, **46**, 3163-3168.

155. D. Peak and T. Z. Regier, *Environ. Sci. Technol.*, 2012, **46**, 6885-6887.

156. D. Peak and T. Z. Regier, *Environ. Sci. Technol.*, 2012, **46**, 11473-11474.

157. A. Manceau, *Environ. Sci. Technol.*, 2012, **46**, 6882-6884.

158. R. K. Hocking, W. P. Gates and J. D. Cashion, *Environ. Sci. Technol.*, 2012, **46**, 11471-11472.

159. D. G. Rancourt and J. F. Meunier, *Am. Mineral.*, 2008, **93**, 1412-1417.

160. A. Manceau, *Clay Minerals*, 2009, **44**, 19-34.

161. F. M. Michel, V. Barrón, J. Torrent, M. P. Morales, C. J. Serna, J. F. Boily, Q. S. Liu, A. Ambrosini, A. C. Cismasu and G. E. Brown, *Proc. Natl. Acad. Sci. U. S. A.*, 2010, **107**, 2787-2792.

162. A. Manceau, *Am. Mineral.*, 2012, **97**, 255-256.

163. F. M. Michel, L. Ehm, S. M. Antao, P. L. Lee, P. J. Chupas, G. Liu, D. R. Strongin, M. A. A. Schoonen, B. L. Phillips and J. B. Parise, *Science*, 2007, **316**, 1726-1729.

164. S. Bashir, R. W. McCabe, C. Boxall, M. S. Leaver and D. Mobbs, *J. Nanopart. Res.*, 2009, **11**, 701-706.

165. S. Réguer, F. Mirambet, E. Dooryhee, J. L. Hodeau, P. Dillmann and P. Lagarde, *Corros. Sci.*, 2009, **51**, 2795-2802.

166. V. A. Drits, B. A. Sakharov, A. L. Salyn and A. Manceau, *Clay Minerals*, 1993, **28**, 185-207.

167. T. Hiemstra and W. H. Van Riemsdijk, *Geochim. Cosmochim. Acta*, 2009, **73**, 4423-4436.

168. A. Manceau, *Am. Mineral.*, 2011, **96**, 521-533.

169. T. Hiemstra, *Geochim. Cosmochim. Acta*, 2013, **105**, 316-325.

170. Z. Y. Wu, A. Mottana, A. Marcelli, E. Paris, G. Giuli and G. Cibin, *Phys. Rev. B*, 2004, **69**, 104106.

171. F. Bourgeois, P. Gergaud, H. Renevier, C. Leclere and G. Feuillet, *J. Appl. Phys.*, 2013, **113**, 013510.

172. J. R. Smyth, *Am. Mineral.*, 1975, **60**, 1092-1097.

173. O. Crisan and A. D. Crisan, *J. Alloys Compd.*, 2011, **509**, 6522-6527.

174. H. Fjellvåg, F. Grønvold, S. Stølen and B. Hauback, *J. Solid State Chem.*, 1996, **124**, 52-57.

175. N. J. Hair and J. K. Beattie, *Inorg. Chem.*, 1977, **16**, 245-250.

176. L. S. Skogareva, G. V. Shilov and A. I. Karelin, *J. Struct. Chem.*, 2012, **53**, 907-914.

177. D. Levy, R. Giustetto and A. Hoser, *Phys. Chem. Min.*, 2012, **39**, 169-176.

178. F. Jiao, A. Harrison, J. C. Jumas, A. V. Chadwick, W. Kockelmann and P. G. Bruce, *J. Am. Chem. Soc.*, 2006, **128**, 5468-5474.

179. L. A. Taylor, H. K. Mao and P. M. Bell, *Geochim. Cosmochim. Acta*, 1974, **Suppl. 5, Vol. 1 (Proceedings of the Fifth Lunar Conference)** 743-748.

180. R. M. Cornell and U. Schwertmann, *The Iron Oxides: Structure, Properties, Reactions, Occurrence and Uses*, Wiley VCH, 2003.

181. H. B. Guo and A. S. Barnard, *J. Mater. Chem. A*, 2013, **1**, 27-42.

182. D. A. Fletcher, R. F. McMeeking and D. Parkin, *J. Chem. Inf. Comput. Sci.*, 1996, **36**, 746-749.

ARTICLE TYPE

How does iron interact with sporopollenin exine capsules? An X-ray absorption study including microfocus XANES and XRF imaging

Stephen J. Archibald,[a] Stephen L. Atkin,[b,c] Wim Bras,[d] Alberto Diego-Taboada,[b,c] Grahame Mackenzie,[a,c] J Frederick W. Mosselmans,[e] Sergey Nikitenko,[d] Paul D. Quinn,[e] Michael F. Thomas[f] and Nigel A.
5 **Young*[a]**

Notes and references

[a] *Department of Chemistry, The University of Hull, Kingston upon Hull, HU6 7RX, U.K.*
10 [b] *Hull York Medical School, The University of Hull, Kingston upon Hull HU6 7RX, U.K.*
[c] *Sporomex Ltd., Newland Avenue, Driffield, YO25 6TX, U.K.*
[d] *DUBBLE@ESRF, BP 220 Grenoble 38143, France*
[e] *Diamond Light Source, Harwell Science and Innovation Campus, Didcot, OX11 0DE, U.K.*
[f] *Department of Physics, University of Liverpool, L69 7ZE, U.K.*

15

Figure 1. SEM images of sporopollenin exine capsules after reaction with FeCl$_3$ solution (left) and FeCl$_2$ solution (right), both air dried.

ARTICLE TYPE
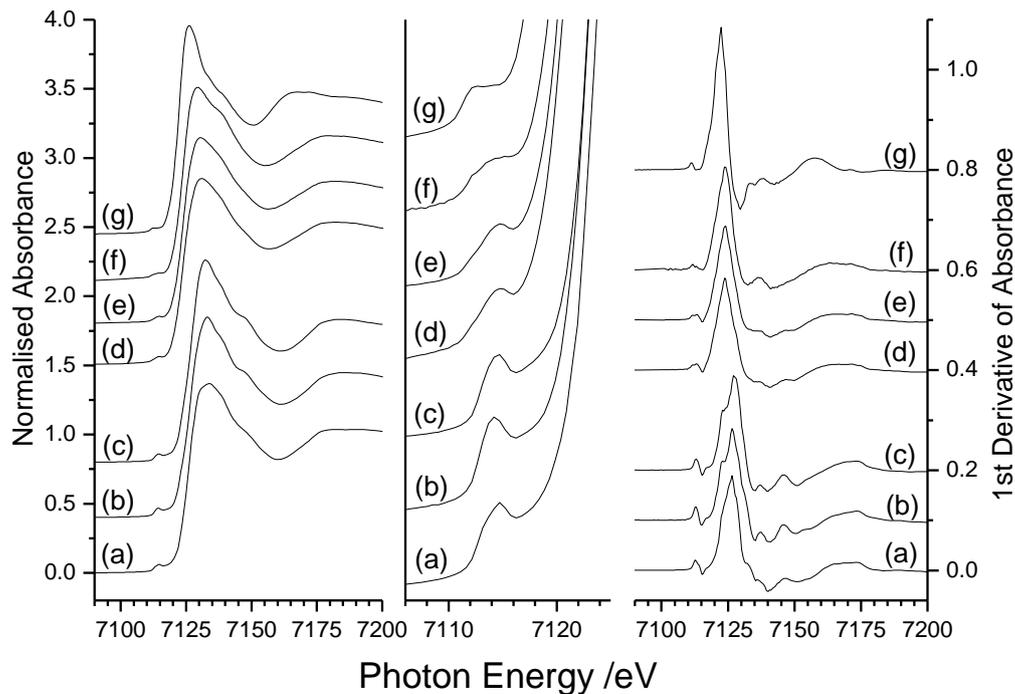
Figure 2. Fe K-edge XANES (left), pre-edge expansion (centre) and 1st derivative (right) spectra of: (a) basic ferric acetate; (b) SEC after reaction with FeCl$_3$ solution and air dried; (c) SEC after reaction with FeCl$_2$ solution and air dried; (d) SEC after reaction with FeCl$_2$ under argon (fresh); (e) SEC after reaction with FeCl$_2$ under argon and ageing in air for 2 weeks; (f) SEC after reaction with Fe(BF$_4$)$_2$ under argon; (g) ferrous acetate.

5

ARTICLE TYPE
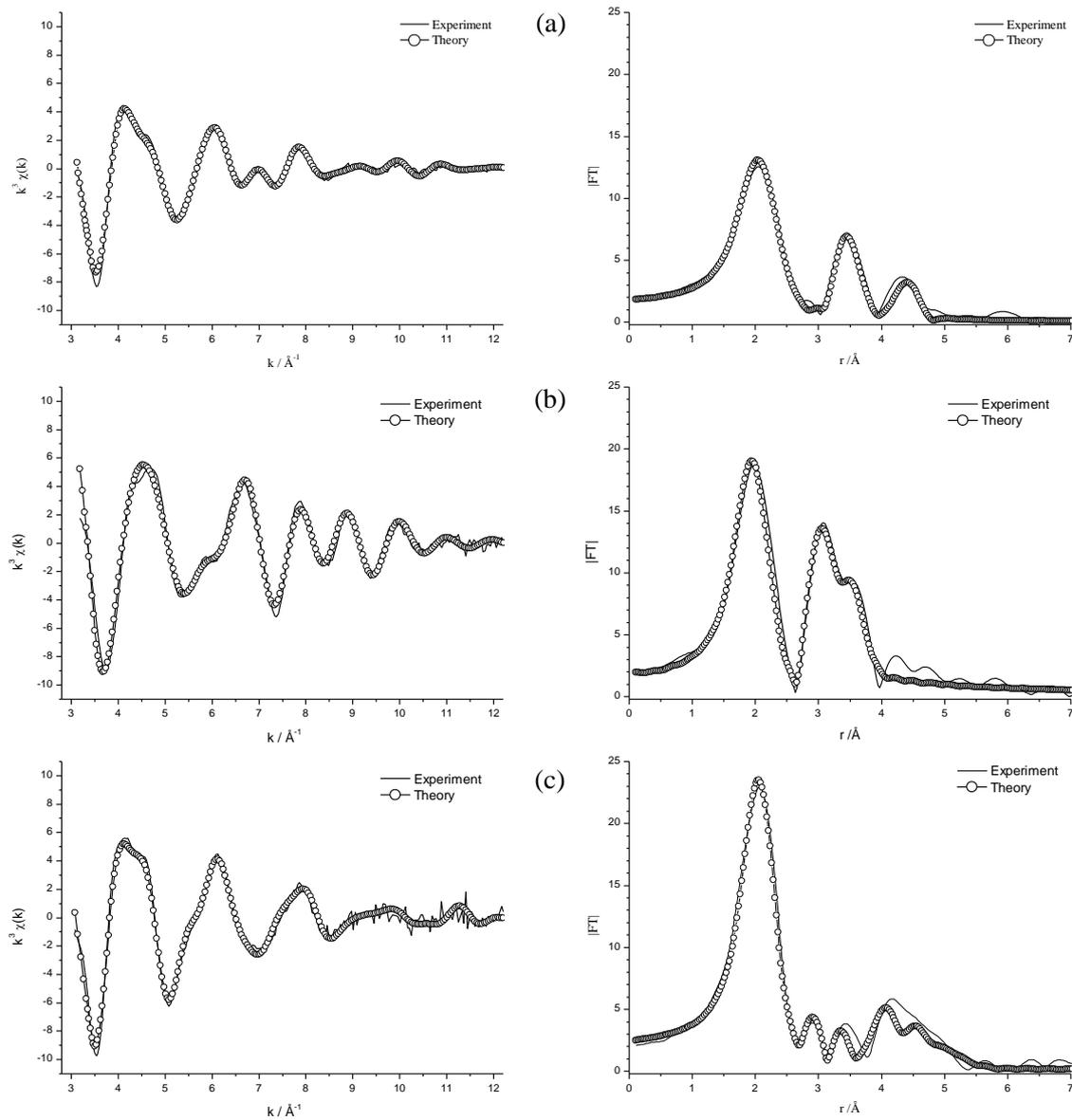
Figure 3. Fe K-edge EXAFS (left) and FTs (right) for (a) ferrous acetate, (b) basic ferric acetate and (c) cobalt acetate tetrahydrate.

5

Table 1. Summary of refined EXAFS parameters for iron and cobalt acetate standards.[a]

	Fe-O$_6$ r /Å [b]	2σ²/Å² [c]	Fe-C$_4$ r /Å	2σ²/Å²	Fe-Fe$_2$ r /Å	2σ²/Å²		
basic ferric acetate	2.016(5)	0.03281(12)	2.982(9)	0.0109(18)	3.358(6)	0.0159(13)		
	E$_f$/V [d] 0.22(37)		FI [e] 0.35		R [f] 23.0			

	Fe-O$_6$ r /Å	2σ²/Å²	Fe-C$_3$ r /Å	2σ²/Å²	Fe-Fe$_2$ r /Å	2σ²/Å²	Fe-C$_2$ r /Å	2σ²/Å²
ferrous acetate	2.133(4)	0.0422(10)	3.157(15)	0.0200(41)	3.332(8)	0.0247(19)	4.502(14)	0.0171(34)
	E$_f$/V -0.66(28)		FI 0.22		R 17.2			

	Co-O$_6$ r /Å	2σ²/Å²	Co-C$_2$ r /Å	2σ²/Å²	Co-O$_2$ r /Å	2σ²/Å²	Co-O$_6$ r /Å	2σ²/Å²	Co-C$_6$ r /Å	2σ²/Å²
cobalt acetate tetrahydrate	2.100(4)	0.0183(7)	3.013(20)	0.0069(35)	3.202(26)	0.0174(72)	4.021(24)	0.0309(72)	4.672(20)	0.0068(47)
	E$_f$/V -1.40(37)		FI 0.23		R 16.7				Co-Co$_2$ r /Å 4.825(23)	2σ²/Å² 0.0164(54)

[a] Refinement standard deviation in parentheses; [b] estimated systematic errors in EXAFS bond lengths are ± 1.5% for well-defined co-ordination shells; [c] Debye-Waller factor; [d] E$_f$ is a single refined parameter to reflect differences in the theoretical and experimental Fermi levels;

[e] $R = \left[\int \left| \chi^T - \chi^E \right| k^3 dk \Big/ \int \left| \chi^E \right| k^3 dk \right] x100\%$ [f] $FI = \sum_i \left[\left(\chi_i^T - \chi_i^E \right) k_i^3 \right]^2$

.
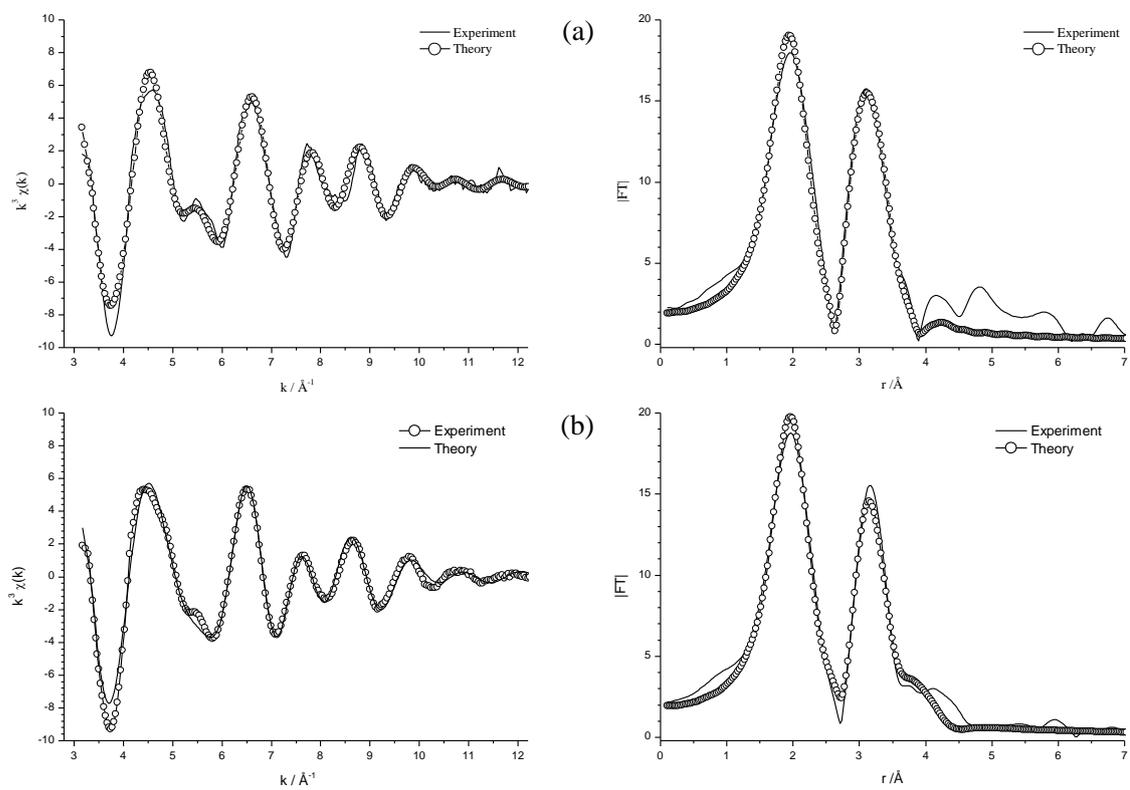
Figure 4. Fe K-edge EXAFS (left) and FT (right) SEC reacted with (a) FeCl$_3$ solution and air dried and (b) FeCl$_2$ solution and air dried.

Table 2. Summary of refined EXAFS parameters for sporopollenin exine capsules after reaction with $FeCl_3$, $FeCl_2$ and $[Fe(BF_4)_2]$ solutions.[a]

	Fe-O$_6$ r /Å [b]	2σ² /Å² [c]	Fe-Fe$_3$ r /Å	2σ² /Å²	Fe-Fe$_3$ r /Å	2σ² /Å²	Fe-Fe$_3$ r /Å	2σ² /Å²
FeCl$_3$ (air dried)	2.010(7)	0.0334(13)	2.990(8)	0.0279(18)	3.422(13)	0.0231(24)	3.667(22)	0.0317(52)
	E$_f$/V [d] −1.40(37)		FI [e] 0.23		R [f] 16.7			
FeCl$_2$ (air dried)	2.022(5)	0.0320(10)	3.062(6)	0.0251(14)	3.458(15)	0.0375(46)	3.902(58)	0.0656(210)
	E$_f$/V −0.85(41)		FI 0.24		R 16.7			
FeCl$_2$ (prepared and stored under Ar)	2.057(4)	0.0399(8)	3.065(13)	0.0489(38)	3.393(13)	0.0421(35)		
	E$_f$/V −2.2(28)		FI 0.20		R 19.3			
FeCl$_2$ (prepared under Ar, exposed to air for two weeks)	2.058(4)	0.0388(8)	3.060(13)	0.0499(38)	3.386(13)	0.0433(36)		
	E$_f$/V −2.1(28)		FI 0.18		R 18.0			
Fe(BF$_4$)$_2$ (prepared and stored under Ar)	2.055(12)	0.0364(24)	3.067(74)	0.0589(201)	3.340(62)	0.0479(164)		
	E$_f$/V −0.95(94)		FI 1.05		R 40.7			

[a] Refinement standard deviation in parentheses; [b] estimated systematic errors in EXAFS bond lengths are ± 1.5% for well-defined co-ordination shells; [c] Debye-Waller factor; [d] E$_f$ is a single refined parameter to reflect differences in the theoretical and experimental Fermi levels;

[e] $R = \left[\int \left| \chi^T - \chi^E \right| k^3 dk \Big/ \int \left| \chi^E \right| k^3 dk \right] x100\%$ [f] $1 \cdot FI = \sum_i \left[\left(\chi_i^T - \chi_i^E \right) k_i^3 \right]^2$

.

ARTICLE TYPE

Figure 5. Fe K-edge EXAFS (left) and FT (right) for SECs reacted with: (a) $FeCl_2$ solution prepared and stored under argon; (b) SECs reacted with $FeCl_2$ solution prepared under argon and stored in air for two weeks (middle); and (c) SECs reacted with $Fe(BF_4)_2$ solution prepared and stored under argon.

ARTICLE TYPE
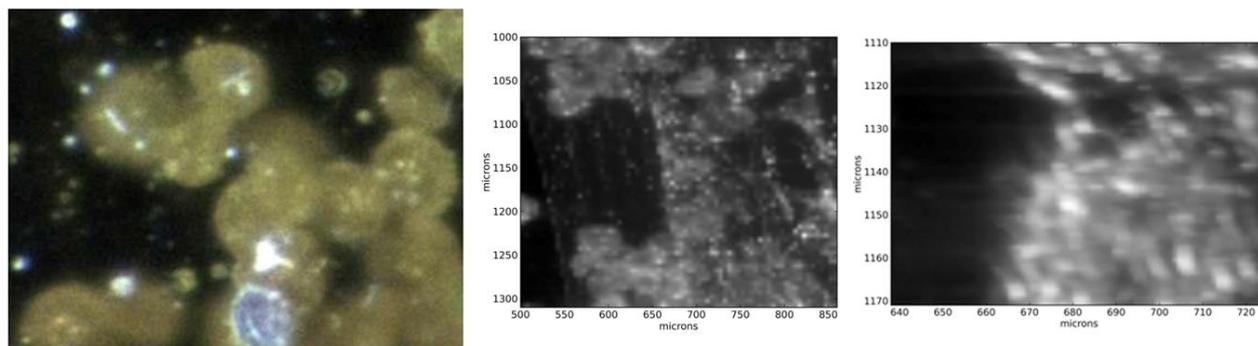
X

Figure 6. SECs reacted with $FeCl_3$ solution and air dried. Left, optical image; centre, Fe K_α XRF map (5 µm pixel size); right Fe K_α XRF map (1 µm pixel size).
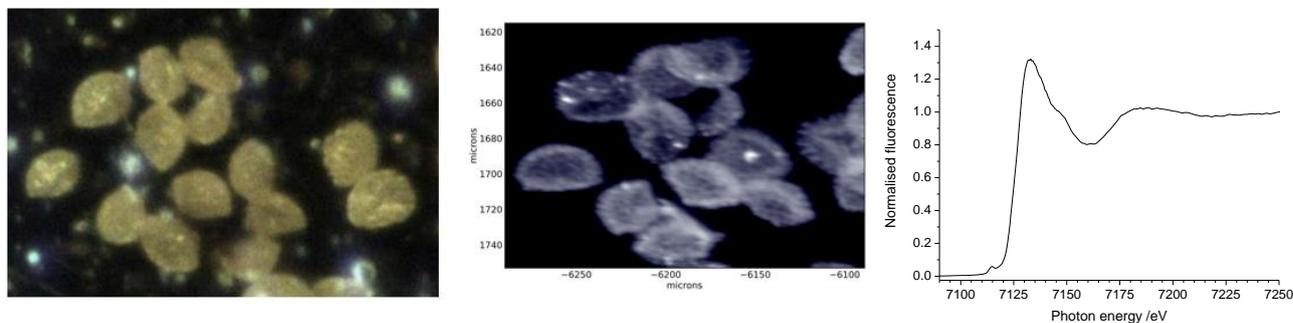
5   **Figure 7**. SECs reacted with $FeCl_2$ solution and air dried. Left, optical image; centre, Fe K_α XRF map (1 µm pixel size); right, Fe K-edge XANES spectrum measured at point −6260, 1695.
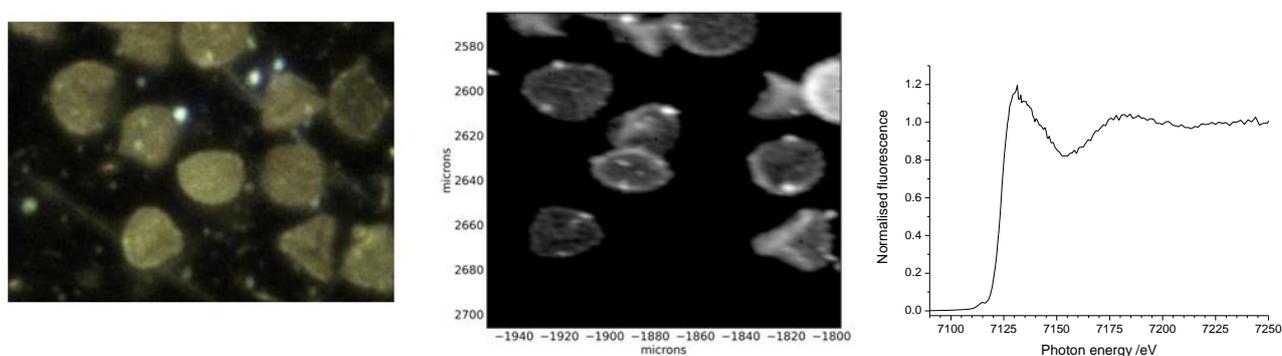
Figure 8. SECs reacted with $FeCl_2$ solution prepared and stored under Ar. Left, optical image; centre, Fe K_α XRF map (1 µm pixel size); right, Fe K-edge XANES spectrum measured at point −1887, 2635.

10